

## Corrosion behavior of a 2304 lean duplex stainless steel cold-rolled and short-term annealed at different temperatures

Raphael França Assumpção<sup>1\*</sup>, Dalila Chaves Sicupira<sup>2</sup>, Dagoberto Brandão Santos<sup>1</sup>

<sup>1</sup>Universidade Federal de Minas Gerais, Departamento de Engenharia Metalúrgica e de Materiais. Belo Horizonte, MG, Brasil.

<sup>2</sup>Universidade Federal de Ouro Preto, Departamento de Química, Campus Morro do Cruzeiro. Ouro Preto, MG, Brasil.  
e-mail: raphaela@ufmg.br, dalila@ufop.edu.br, dsantos@demet.ufmg.br

### ABSTRACT

This study examined the effects of cold working and subsequent annealing treatment for a short time on the corrosion behavior of a lean duplex stainless steel (LDSS). The as-received sample was solution treated at 1100 °C for 1800 s and cold rolled. The cold deformation (75%) was followed by isochronic annealing at 900, 950, 1000, 1050 and 1100 °C for 180 s. The microstructural changes were evaluated by scanning electron microscopy (SEM) and Vickers hardness, while corrosion behavior was investigated by cyclic potentiodynamic polarization technique and electrochemical impedance spectroscopy (EIS) in 3.5% NaCl solution at  $22 \pm 2$  °C. After cyclic polarization, pits morphology was characterized by SEM. Cold rolling lowered lamellar spacing between the phases and increased hardness. Hardness at temperatures higher than 950 °C was equal to the 2304 LDSS solution treated. Although grain refinement is observed due to recrystallization, the corrosion resistance was not significantly improved. The highest pitting potential and charge transfer resistance were obtained after annealing at 1000 °C for 180 s. The pit distribution indicates that the corrosion behavior of the phases changed during the cold rolling and annealing treatment, and pitting was initiated preferentially in the  $\alpha/\gamma$  boundaries and inside the  $\alpha$  domains.

**Keywords:** lean duplex stainless steel; pitting corrosion; short-term annealing.

### 1. INTRODUCTION

Lean Duplex stainless steels (LDSS), characterized by a dual-phase austenitic-ferritic microstructure, offer attractive combinations of mechanical properties and corrosion resistance at a reasonable cost compared with conventional DSS grades due to a lower content of elements such as NI and MO [1]. Annealing temperature strongly influences the corrosion resistance of the ferrite and austenite phases, so there is an optimum temperature where the two phases behave similarly [2]. According to BREDA *et al.* [3], changes in annealing temperature influence the passive film thickness and its protective behavior.

ZHANG *et al.* [4] evaluated the effect of annealing temperature on the pitting corrosion resistance of 2101 lean duplex stainless steel by potentiodynamic polarization curves carried out in 1 mol L<sup>-1</sup> NaCl solution. Increasing the annealing temperature from 1000 °C to 1200 °C shifted the corrosion potential ( $E_{\text{corr}}$ ) and the pitting potential ( $E_{\text{pit}}$ ) to more negative values, weakening the pitting corrosion resistance of the material. Similar procedures were adopted by ZHANG *et al.* [5] to correlate the annealing temperature and the pitting resistance of 2304 lean duplex steel. It was found that the values of  $E_{\text{pit}}$  became more positive with increasing annealing temperature from 1000 °C to 1080 °C and then became more negative from 1100 °C to 1200 °C.

Cold working considerably affects the pitting resistance of stainless steels because of residual stress and the possible formation of the strain-induced  $\alpha'$ -martensite (SIM) from the metastable austenite [6]. Using plastic deformation to induce martensitic transformation in LDSS and then reverting the martensite to austenite through annealing can lead to grain refinement [7]. LV *et al.* [6], in their studies about a 2205 alloy, observed that grain refinement reduced the passive current, increased pitting corrosion potential, and improved corrosion resistance.

This work aims to contribute to the effect of solution treatment and short-term annealing at different temperatures, aimed at grain refining, on the corrosion behavior of an LDSS 2304 in 3,5% NaCl. For this purpose, the LDSS 2304 was cold rolled up to 75% and subsequently annealed at 900 °C to 1100 °C for 180 s.

**Table 1:** Chemical composition of 2304 lean duplex stainless steel (in wt.%).

C	Cr	Ni	Mo	Mn	Si	P	Cu	S	N
0.011	22.87	4.20	0.275	1.45	0.201	0.02	0.453	0.0004	0.101

## 2. MATERIALS AND METHODS

This study was carried out using 4 mm thick sheets of hot-rolled 2304 lean duplex stainless. The steel chemical composition analyzed by mass spectroscopy is given in Table 1.

The as-received samples (AR) underwent a solution treatment (AR-ST) step at 1100 °C for 1800 s. The AR-ST sheets were cold rolled in a Fröhling laboratory rolling mill at 6.5 m/min, achieving a thickness reduction of 75% in 14 passes. Then, the cold rolled samples were isochronic annealed at 900 °C, 950 °C, 1000 °C, 1050 °C and 1100 °C for 180 s and water quenched. The thickness reduction and annealing time were selected based on the literature aiming at grain refining [8].

The samples for the microstructural analysis were characterized along the longitudinal section using scanning electron microscopy (SEM). The samples were ground with SiC abrasive papers with grit up to 1000#, polished with fine diamond paste (9, 6, and 1 µm), and then etched with Beraha etchant. Microhardness Vickers (HV-dwell time of 10 s and a load of 300 gf) was measured using a Future Tech FM-700 microhardness tester. The mean HV values for each sample were calculated from twenty random measurements along the thickness plane.

The electrochemical measurements were performed with a potentiostat Autolab PGSTAT302N using a three-electrode cell. A platinum plate and an Ag/AgCl (sat.) were used as the counter and the reference electrodes, respectively. The specimens acting as working electrodes were embedded in acrylic resin. The contact region between the sample and the acrylic resin was sealed with Araldite epoxy adhesive to avoid the occurrence of crevices.

For the electrochemical analysis, DSS plates were cut in 10 mm × 10 mm, grounded with SiC paper up to 600#, cleaned in ethanol and distilled water, and dried in air. The electrochemical measurements were conducted in 3.5% NaCl at 22 ± 2 °C and initiated after 60 min at the open circuit potential (OCP) stabilization. A minimum of three measurements for each sample were taken to ensure good reproducibility, and an average value was considered.

Potentiodynamic anodic polarization experiments were performed to determine the anodic potential range for passive film formation. A scan rate of 1.0 mV s<sup>-1</sup> was used in the anodic direction, starting from the open-circuit potential, OCP, to the potential at which the current density reached 1.0 mA cm<sup>-2</sup>. EIS tests were carried out at open-circuit potential conditions and AC potential with the amplitude of 10 mV and frequency range of 100 kHz to 5 mHz. The acquired impedance spectra are presented as Nyquist plots and interpreted in terms of equivalent electrical circuits using the ZView (Scribner Assoc.) program.

## 3. RESULTS AND DISCUSSION

Figure 1 shows scanning electron micrographs (SEM) of the samples as-received (AR), solution-treated (AR-ST) and cold-rolled (CR) with 75% thickness reduction. The contrast between the phases in the SEM images was not so pronounced. However, phase identification can be made through relief. The Beraha reagent used preferentially attacks the ferrite, emphasizing the austenite.

Hot rolling (Figure 1a) resulted in a partial work-hardened with elongated grains along the rolling direction. Both phases developed a typical lamellar structure called pancake structure, consisting of alternating lamellas of austenite and ferrite. After the solution annealing treatment (Figure 1b), it was observed that austenite bands were incorporated in the ferrite matrix since the growth and coalescence of the grains of the two phases occurred. Furthermore, a lack of continuity in the austenite lamellae indicates that part of the austenitic phase is transformed into ferrite and that the ferritic grains grew as the austenite lamellae were consumed. Cold rolling (Figure 1c) resulted in a considerable decrease in lamellae spacing.

Figure 2 shows the microstructure of the cold-rolled and subsequently annealed for 180 s at temperatures of 950 °C, 1000 °C and 1050 °C. After isothermal annealing at 950 °C (Figure 2a), a slight increase in austenite lamellae thickness and austenite inside ferrite lamellas was observed compared to the cold rolled condition (Figure 1c). The elongated microstructure with alternated austenite and ferrite lamellae remained.

The increase of 50 °C in temperature (Figure 2b) resulted in the bamboo-type morphology. According to PAN *et al.* [9], the grain boundaries ran perpendicular to the phase boundaries, and the grains extended through the full height of the respective layer. Therefore, the austenite grains are recrystallized and grow, although the

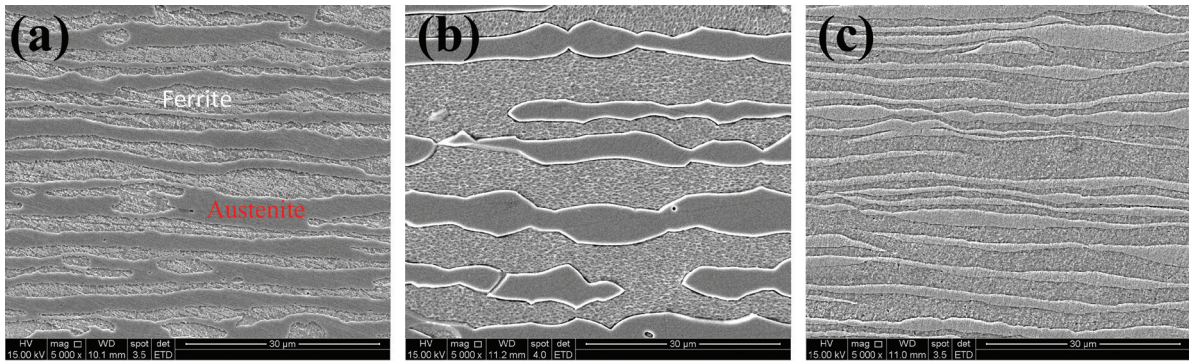


Figure 1: Micrographs obtained via SEM after Beraha etching of the 2304 LDSS specimens: (a) as-received, (b) solution-treated and (c) cold-rolled.

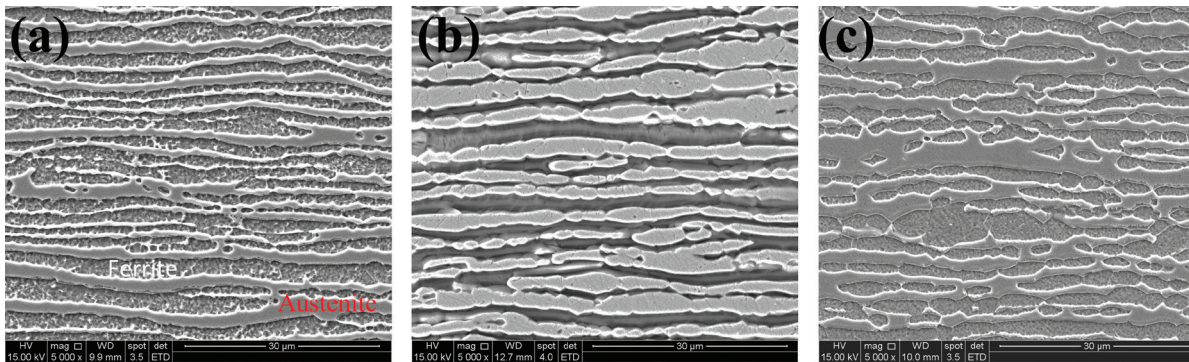


Figure 2: Microstructures of the sample at (a) 950 °C, (b) 1000 °C and (c) 1050 °C for 180 s.

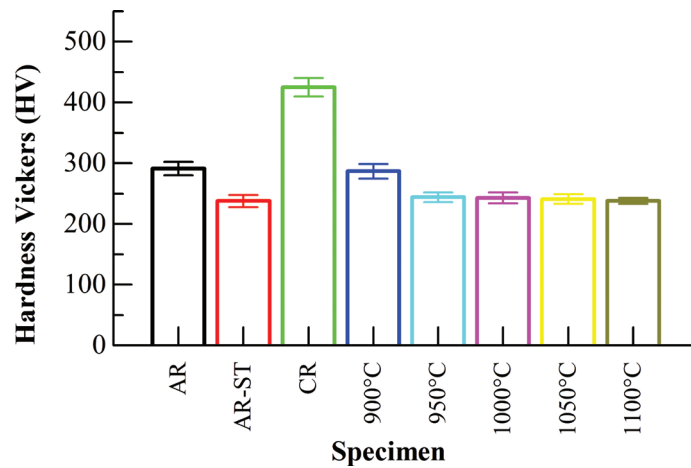


Figure 3: Vickers microhardness of the 2304 duplex stainless steel after annealing at different temperatures.

ferrite lamellae and the neighbor austenite phase boundaries prevent excessive growth. The bamboo-like structure began to break down at 1050 °C (Figure 2c), but no coarsening was observed.

Vickers microhardness values for all conditions was plotted in Figure 3. Solution treatment induced lamellae coarsening (Figure 1a,b) and consequent softening. A hardening mechanism was observed for the 2304 LDSS after cold rolling. The hardness increase is related to work hardening and strain-induced martensite ( $\alpha'$ ) formation from the metastable austenite. SANDIM *et al.* [10] cold-rolled up to 80% thickness reduction an LDSS 2304 and obtained a 0.26 volume fraction of martensite and a hardness of 450 HV.

After annealing at 900 °C, there was a clear decrease in hardness related to recovery, recrystallization and austenite formed from reversion. The  $\alpha'$ -martensite reversion transformation occurs at temperatures well below the austenitic recrystallization temperature. SANDIM *et al.* [10] reported that annealing at 800 °C leads

to complete austenite reversion. SANTOS *et al.* [7] study with a 2304 LDSS with 60% thickness reduction indicated that at 900 °C, the steel would be fully recrystallized after 30 min. Increasing the temperature from 950 °C to 1100 °C did not significantly change the microhardness. MOURA *et al.* [11] associated the hardness stability with the absence of significant recrystallization progress.

Figure 4 shows typical cyclic potentiodynamic polarization (CPP) curves of the samples in a 3.5% NaCl solution. The backward polarization (Figure 4) showed a positive hysteresis, a large hysteresis loop and did not intersect the passive region in the forward scan. Some of the curves in the reverse scans cross the forward scan at values similar to OCP, which indicate that pitting corrosion might occur over long periods of OCP exposure to the 3.5% NaCl solution [12].

The passive current density increased with increasing potential for the treated samples but remained on the order of  $10^{-6}$  A/cm<sup>2</sup>. The mean pitting potential (E<sub>pit</sub>) and its standard deviation obtained from the polarization tests are shown in Figure 5.

Figure 5 indicates that pitting potential decreases after cold rolling of the AR-ST samples. A slight increase in pitting potential is observed after annealing for 900 °C–1000 °C. However, no improvement was

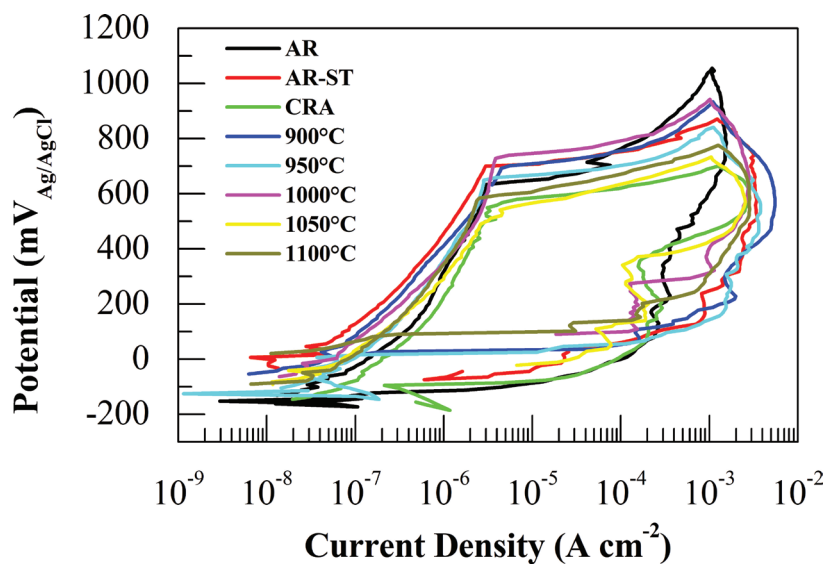


Figure 4: Typical cyclic potentiodynamic polarization curves for all conditions studied.

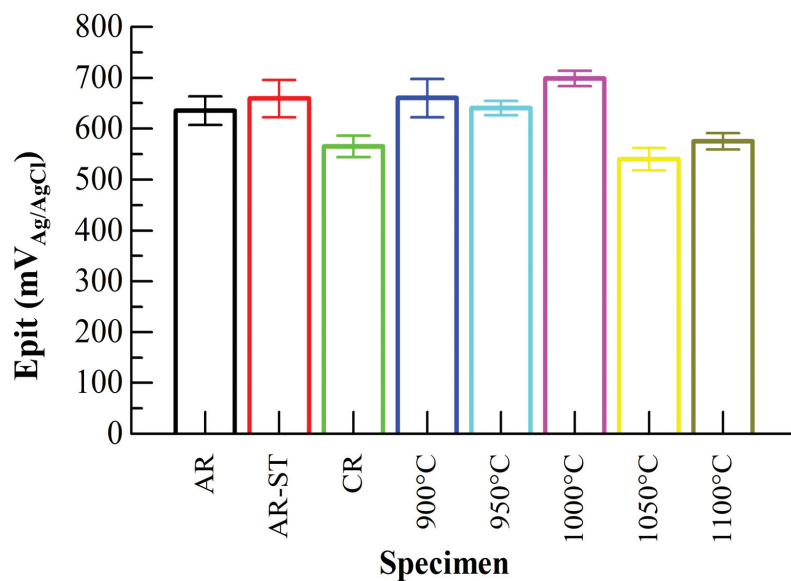


Figure 5: Experimental data for pitting corrosion potential obtained by cyclic polarization tests.

observed for the samples annealed at 1050 °C and 1100 °C. The pitting potential is lowered at 1050 °C, where the recrystallization phenomenon is in an advanced state (Figure 2).

JINGLONG *et al.* [13] evaluated the effect of grain refinement on the corrosion resistance of passive film formed on 2205 DSS in a borate buffer solution. The as-received steel was annealed at 1100 °C for 1 h and water-quenched to produce coarse-grained steel. The ultrafine grained was obtained by cold rolling the coarse-grained condition with 95% thickness reduction and annealed at 900 °C up to 200 s. The results indicate that the ultragrained DSS showed a higher corrosion resistance than the coarse-grained owing to a thicker passive film enriched in Cr<sub>2</sub>O<sub>3</sub> with low defect density [13].

ZHANG *et al.* [4] reported with an as-received 2101 LDSS annealed at 1000 °C to 1200 °C for 1800 s that the pitting potential in 1 mol L<sup>-1</sup> NaCl decreased with increasing temperature, along with a decrease of austenite volume fraction. TAN *et al.* [14] study indicates that short-time annealing for 240 s at different temperatures ranging from 1020 °C to 1120 °C had a beneficial effect on pitting corrosion resistance in 1 mol L<sup>-1</sup> NaCl solution due to an increase in austenite fraction.

MALTA *et al.* [8] studied a 2304 LDSS cold rolled (75%) without the solution treatment step, and there was a decrease in pitting corrosion after annealing at 900 °C and 950 °C for 180 s compared to the cold rolled sample. However, the corrosion resistance shifts to values close to the CR at temperatures from 1000 °C to 1100 °C, being the best resistance to pitting corrosion at the 1000 °C annealed condition. The increasing temperature decreased the austenite volume fraction, but austenite's PREN (pitting resistance number) increased.

Figures 6 and 7 illustrates the morphology of the pits formed after the CPP test. An electron backscatter detector obtained a chemical contrast between the ferrite (dark gray) and the austenite phase (light gray). In the cold-rolled samples (Figure 6b), the pits were formed in greater quantity when compared with the hot-rolled samples (Figure 6a).

In the solution-treated and cold-rolled samples (Figure 6), most pits tend to nucleate at the  $\alpha/\gamma$  interface. Nonetheless, pitting is found inside the  $\gamma$  phase in the solution-treated sample and the inside  $\alpha$  phase in the cold-rolled. The pit distribution indicates that the corrosion behavior of the phases changed with the cold rolling, and ferrite became the less resistant phase.

At 900 °C (Figure 7a), pitting was initiated preferentially in the  $\alpha/\gamma$  boundaries and inside the  $\alpha$  domains, indicating that the  $\alpha$  phase had low pitting corrosion resistance as compared to the  $\gamma$  phase. The same trend can be observed at 900 °C to 1050 °C (Figure 7a–d). At 1100 °C, Figure 7e, pits are distributed within the austenite and ferrite phases, indicating similar corrosion behavior.

Figure 8 shows the Nyquist and Bode plots for the 2304 LDSS AR, AR-ST, CR and annealed from 900 °C to 1100 °C for 180 s. The Nyquist diagram, Figure 8a, shows the correlation between real and imaginary impedance at each frequency. Figure 8b shows high phase angle values over a wide frequency range. As seen in Figure 8b, the Bode diagram has a one-time constant (only a maximum at the phase angle in the mid-frequency region).

Differences in the semicircle arcs can be observed for the specimens in Nyquist plots. The diameter of the capacitive semicircle arc indicates the corrosion resistance of the passive films, and the larger diameter indicates the passive film's higher corrosion resistance [15]. There was no clear trend in the diameter of the depressed semicircle with increasing temperature. The samples AR-ST, CR and annealed at 1100 °C presented the smallest semicircle diameters, implying reduced corrosion resistance of the passive film in 3.5 NaCl and OCP conditions.

The Bode graphs in Figure 8b showed a sloped impedance modulus and a defined maximum phase angle at medium frequencies, presenting a capacitive behavior. It is observed in high frequency, with a tendency for a phase angle close to 0, indicating a resistor behavior of the rust layer at high frequency. For the sample annealed at 1050 °C, the phase angle shift to lower frequencies compared to the other samples.

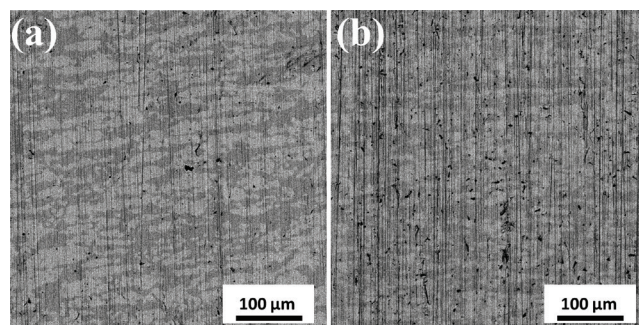


**Figure 6:** Pit morphologies after polarization measurements of the 2304 LDSS: (a) solution-treated and (b) cold-rolled.

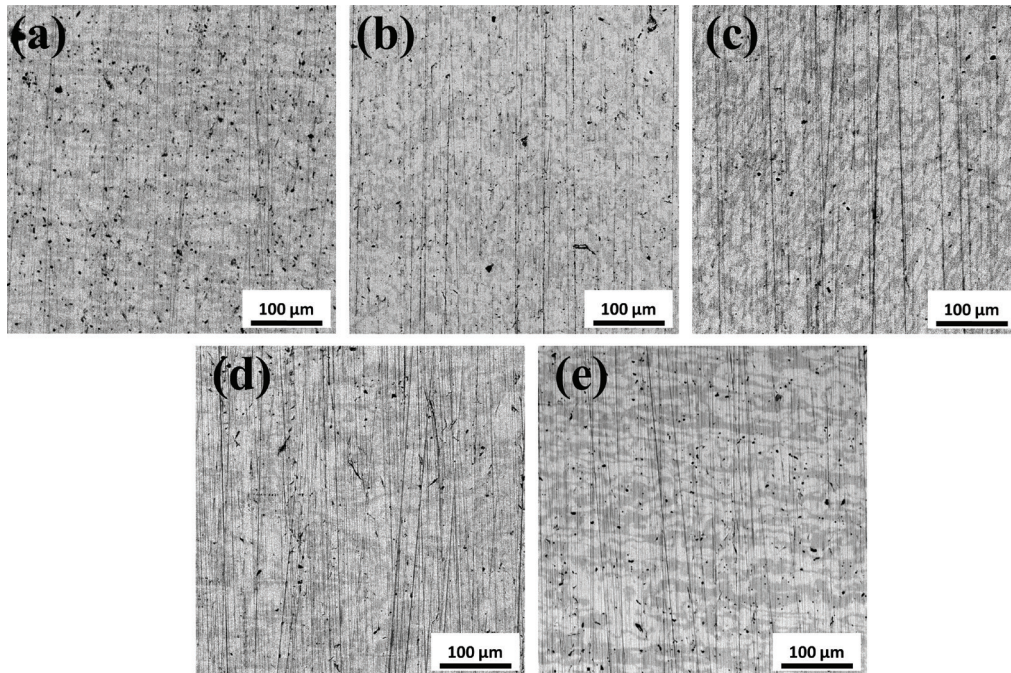


Figure 7: SEM images of metastable pits formed on the specimens annealed at (a) 900 °C, (b) 950 °C, (c) 1000 °C, (d) 1050 °C and (e) 1100 °C for 180 s after the cyclic polarization test.

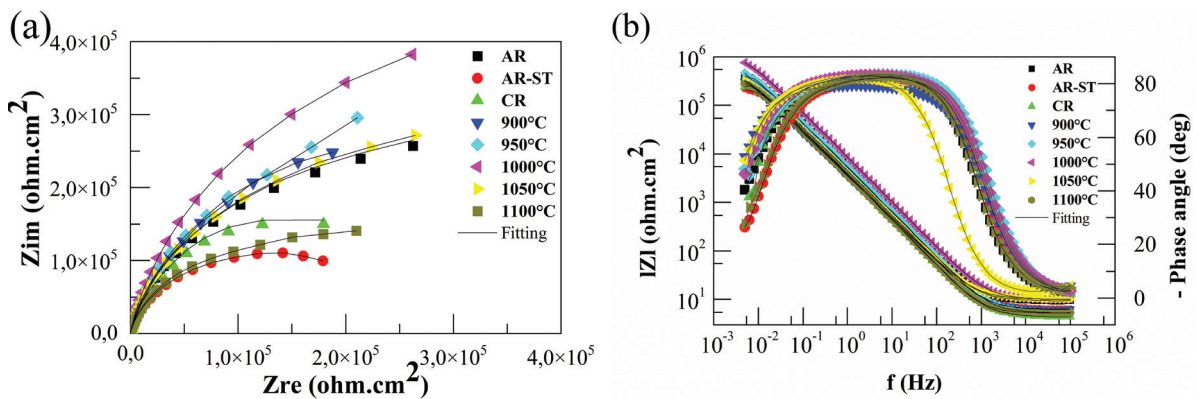


Figure 8: (a) Nyquist plots and (b) Bode phase plots of passive films formed in 3.5% NaCl solution for the 2304 LDSS.

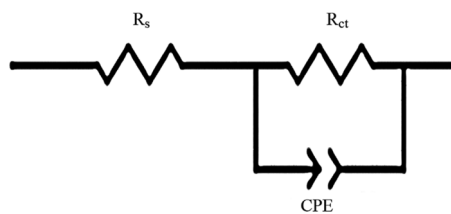


Figure 9: Equivalent circuits diagram used to model the impedance data.

The equivalent circuit in Figure 9 is proposed for fitting EIS data to quantify the electrochemical parameters on 2304 LDSS [16–18]. In this equivalent circuit,  $R_s$  represents solution resistance; CPE is the constant phase element and capacitance, and  $R_{ct}$  is the charge transfer resistance at the metal/electrolyte interface. The mean values of the fitting parameters of EIS data are shown in Table 2.

**Table 2:** Electrochemical parameters fitted based on EIS spectra of the 2304 LDSS samples in a 3.5% NaCl solution.

SAMPLE	$R_s (\Omega \text{ cm}^2)$		$R_{ct} (\Omega \text{ cm}^2)$		$Q (\Omega^{-1} \text{ cm}^{-2} \text{ s}^n)$		$n$	
	VALUE	DEVIATION	VALUE	DEVIATION	VALUE	DEVIATION	VALUE	DEVIATION
AR	8.1	1.4	5.87E+05	3.70E+04	4.23E-05	4.15E-06	0.917	0.002
AR-ST	6.3	0.2	2.22E+05	4.13E+04	4.52E-05	4.08E-06	0.912	0.001
CR	4.8	0.4	3.74E+05	4.10E+02	4.88E-05	1.94E-06	0.922	0.001
900°C	6.2	1.2	7.25E+05	4.20E+04	3.36E-05	1.98E-06	0.922	0.004
950°C	6.1	0.9	7.25E+05	4.20E+04	3.36E-05	1.98E-06	0.922	0.004
1000°C	7.7	0.4	9.97E+05	3.91E+04	2.69E-05	1.58E-06	0.918	0.001
1050°C	6.2	0.1	6.45E+05	7.22E+04	3.99E-05	2.72E-06	0.912	0.008
1100°C	8.3	1.1	3.52E+05	6.81E+04	4.58E-05	8.59E-06	0.918	0.004

It is observed that the solution heat treatment did not favor the passive film resistance of the 2304 LDSS. The solution treatment temperature may dilute key alloying elements between the phases and change the passive film behavior. A slight increase in  $R_{ct}$  is observed after cold deformation. It is reported that cold working could improve the passive film corrosion resistance owing to a more compact and dense passive film [6]. After annealing,  $R_{ct}$  increases up to 1000 °C and slightly decreases. This may be related to grain growth, alloying elements diffusion and a decrease in austenite volume fraction [4,8]. A similar tendency is observed with pitting potential in Figure 5.

#### 4. CONCLUSIONS

The band-like morphology of the as-received specimen coarsened with the solution heat treatment and was replaced by a pancake structure after cold rolling. Cold rolling promoted a reduction in the phase spacing accompanied by increased dislocation density and possible  $\alpha'$ -martensite formation. After annealing, a considerable decrease in lamellae spacing was observed. Microhardness remarkably increases with cold rolling. After annealing, microhardness decreases due to a softening mechanism promoted by recovery and recrystallization phenomena.

Although grain refining was observed after annealing at temperatures ranging from 900 °C–1100 °C for 180 s, no significant pitting corrosion resistance improvement was observed. Pitting was initiated preferentially in the  $\alpha/\gamma$  boundaries and inside the  $\alpha$  domains. The pit distribution indicates that the corrosion behavior of the phases changed during the thermomechanical treatment.

EIS results showed differences in the semicircle arcs for the specimens in the Nyquist plots. The highest charge transfer resistance was found after annealing the cold rolled sample at 1000 °C for 180 s. At this temperature, the pitting potential was also the highest.

#### 5. ACKNOWLEDGMENTS

The authors are grateful to CAPES-PROEX, CNPq and FAPEMIG for the research fellowships made available to students and for their financial support. Thanks are expressed to Aperam South America SA for the samples supplied.

#### 6. BIBLIOGRAPHY

- [1] LO, K.H., SHEK, C.H., LAI, J.K.L., “Recent developments in stainless steel”, *Materials Science and Engineering R Reports*, v. 65, n. 4–6, pp. 39–104, 2009. doi: <http://dx.doi.org/10.1016/j.mser.2009.03.001>.
- [2] GUO, Y., HU, J., LI, J., *et al.*, “Effect of annealing temperature on the mechanical and corrosion behavior of a newly developed novel lean duplex stainless steel”, *Materials*, v. 7, n. 9, pp. 6604–6619, 2014. doi: <http://dx.doi.org/10.3390/ma7096604>. PubMed PMID: 28788201.
- [3] BREDI, M., PEZZATO, L., PIZZO, M., *et al.*, “Effect of cold rolling on pitting resistance in duplex stainless steels”, *La Metallurgia Italiana*, v. 106, pp. 15–19, 2014.
- [4] ZHANG, L., ZHANG, W., JIANG, Y., *et al.*, “Influence of annealing treatment on the corrosion resistance of lean duplex stainless steel 2101”, *Electrochimica Acta*, v. 54, n. 23, pp. 5387–5392, 2009. doi: <http://dx.doi.org/10.1016/j.electacta.2009.04.023>.
- [5] ZHANG, Z., HAN, D., JIANG, Y., *et al.*, “Microstructural evolution and pitting resistance of annealed lean duplex stainless steel UNS S32304”, *Nuclear Engineering and Design*, v. 243, pp. 56–62, 2012. doi: <http://dx.doi.org/10.1016/j.nucengdes.2011.11.030>.

- [6] JINLONG, L., TONGXIANG, L., CHEN, W., *et al.*, “Effect of ultrafine grain on tensile behaviour and corrosion resistance of the duplex stainless steel”, *Materials Science and Engineering C*, v. 62, pp. 558–563, 2016. doi: <http://dx.doi.org/10.1016/j.msec.2016.02.008>. PubMed PMID: 26952459.
- [7] SANTOS, R.M., RODRIGUES, D.G., DIAS SANTOS, M.L., *et al.*, “Martensite reversion and strain hardening of a 2304 lean duplex stainless steel subjected to cold rolling and isochronous annealing at low temperatures”, *Journal of Materials Research and Technology*, v. 16, pp. 168–186, 2022. doi: <http://dx.doi.org/10.1016/j.jmrt.2021.11.122>
- [8] MALTA, P.O., CONDÉ, B.L., ASSUMPÇÃO, R.F., *et al.*, “Effect of annealing temperature on mechanical behavior, pitting resistance and grain boundary character of a 2304 lean duplex stainless steel”, *Metallurgical and Materials Transactions. A, Physical Metallurgy and Materials Science*, v. 50, n. 6, pp. 2665–2677, 2019. doi: <http://dx.doi.org/10.1007/s11661-019-05193-1>
- [9] PAN, M., ZHANG, X., CHEN, P., *et al.*, “The effect of chemical composition and annealing condition on the microstructure and tensile properties of a resource-saving duplex stainless steel”, *Materials Science and Engineering A*, v. 788, pp. 139540, 2020. doi: <http://dx.doi.org/10.1016/j.msea.2020.139540>.
- [10] SANDIM, M.J.R.R., SOUZA FILHO, I.R., MOTA, C.F.G.S., *et al.*, “Microstructural and magnetic characterization of a lean duplex steel: Strain-induced martensite formation and austenite reversion”, *Journal of Magnetism and Magnetic Materials*, v. 517, pp. 167370, 2021. doi: <http://dx.doi.org/10.1016/j.jmmm.2020.167370>
- [11] MOURA, A.N., OLIVEIRA, T.R., ANTÔNIO, M., *et al.*, “Study of the recrystallization and crystallographic texture evolution during final annealing of UNS S32304 Lean Duplex stainless steel”, *Materials Characterization*, v. 130, pp. 39–49, 2017. doi: <http://dx.doi.org/10.1016/j.matchar.2017.05.025>
- [12] SICUPIRA, D.C., JUNIOR, R.C., BRACARENSE, A.Q., *et al.*, “Cyclic polarization study of thick welded joints of lean duplex stainless steel for application in biodiesel industry”, *Materials Research*, v. 20, n. 1, pp. 161–167, 2016. doi: <http://dx.doi.org/10.1590/1980-5373-mr-2016-0370>
- [13] JINLONG, L., TONGXIANG, L., CHEN, W., *et al.*, “Comparison of corrosion properties of passive films formed on coarse grained and ultrafine grained AISI 2205 duplex stainless steels”, *Journal of Electroanalytical Chemistry (Lausanne, Switzerland)*, v. 757, pp. 263–269, 2015. doi: <http://dx.doi.org/10.1016/j.jelechem.2015.09.036>
- [14] TAN, H., WANG, Z., JIANG, Y., *et al.*, “Annealing temperature effect on the pitting corrosion resistance of plasma arc welded joints of duplex stainless steel UNS S32304 in 1.0M NaCl”, *Corrosion Science*, v. 53, n. 6, pp. 2191–2200, 2011. doi: <http://dx.doi.org/10.1016/j.corsci.2011.02.041>
- [15] CAO, C., “On the impedance plane displays for irreversible electrode reactions based on the stability conditions of the steady-state—I. One state variable besides electrode potential”, *Electrochimica Acta*, v. 35, n. 5, pp. 831–836, 1990. doi: [http://dx.doi.org/10.1016/0013-4686\(90\)90077-D](http://dx.doi.org/10.1016/0013-4686(90)90077-D)
- [16] SICUPIRA, D.C., CARDOSO JUNIOR, R., BRACARENSE, A.Q., *et al.*, “Electrochemical study of passive films formed on welded lean duplex stainless steel”, *Mater Corros*, v. 68, pp. 604–612, 2017. doi: <http://dx.doi.org/10.1002/maco.201609301>.
- [17] SHI, J., WU, M., MING, J., “Degradation effect of carbonation on electrochemical behavior of 2304 duplex stainless steel in simulated concrete pore solutions”, *Corrosion Science*, v. 177, pp. 109006, 2020. doi: <http://dx.doi.org/10.1016/j.corsci.2020.109006>
- [18] SHANG, B., MA, Y., MENG, M., *et al.*, “Feasibility of utilizing 2304 duplex stainless steel rebar in seawater concrete: passivation and corrosion behavior of steel rebar in simulated concrete environments”, *Mater Corros*, v. 70, n. 9, pp. 1657–1666, 2019. doi: <http://dx.doi.org/10.1002/maco.201910807>